

Silence is Golden: Leveraging Adversarial Examples to Nullify Audio Control in LDM-based Talking-Head Generation

Yuan Gan¹, Jiaxu Miao^{2*}, Yunze Wang³, Yi Yang¹

¹ReLER, CCAI, Zhejiang University

²School of Cyber Science and Technology, Sun Yat-sen University

³Department of Statistics, University of Wisconsin–Madison

Abstract

Advances in talking-head animation based on Latent Diffusion Models (LDM) enable the creation of highly realistic, synchronized videos. These fabricated videos are indistinguishable from real ones, increasing the risk of potential misuse for scams, political manipulation, and misinformation. Hence, addressing these ethical concerns has become a pressing issue in AI security. Recent proactive defense studies focused on countering LDM-based models by adding perturbations to portraits. However, these methods are ineffective at protecting reference portraits from advanced image-to-video animation. The limitations are twofold: 1) they fail to prevent images from being manipulated by audio signals, and 2) diffusion-based purification techniques can effectively eliminate protective perturbations. To address these challenges, we propose **Silencer**, a two-stage method designed to proactively protect the privacy of portraits. First, a nullifying loss is proposed to ignore audio control in talking-head generation. Second, we apply anti-purification loss in LDM to optimize the inverted latent feature to generate robust perturbations. Extensive experiments demonstrate the effectiveness of **Silencer** in proactively protecting portrait privacy. We hope this work will raise awareness among the AI security community regarding critical ethical issues related to talking-head generation techniques. Code: <https://github.com/yuangan/Silencer>.

1. Introduction

Talking-head animation [3, 15, 20, 50, 54, 62, 66, 67] enables the creation of synchronized and highly realistic facial expressions based on audio and portrait images, producing videos that are often indistinguishable from authentic visual recordings. Recent advances in diffusion models [5, 8, 24, 36, 57] have markedly improved the real-

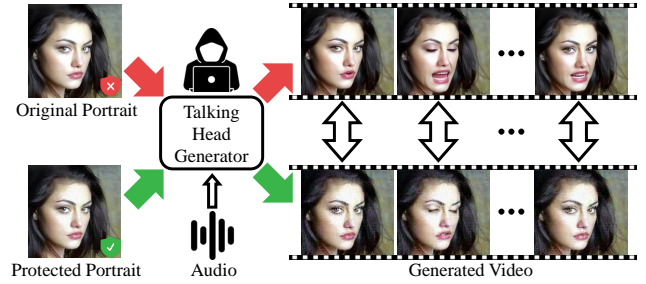


Figure 1. **Overview of Our Motivation.** Given an audio input, talking-head animation models can be exploited to generate fabricated videos using any portrait. To safeguard portrait privacy, we introduced **Silencer**, applying protective perturbations to ensure the portrait’s mouth remains closed in generated talking videos.

ism of these animations. Consequently, this technological advancement increases the risks of misusing AI-Generated Content (AIGC) for scams, political manipulation, and misinformation. Mitigating these ethical risks has become a critical priority in AIGC security.

To address the ethical risks associated with AIGC, there are two primary approaches: passive defenses [9, 37, 44, 49, 60] and proactive defenses [28–30, 38, 40, 59]. Passive defenses focus on detecting whether a video has been fabricated, making it useful for forensics. However, these approaches cannot prevent the infringement of personal privacy by deepfakes. When victims realize their privacy has been violated, the damage may already be irreparable. In contrast, proactive defenses offer superior protection by proactively shielding individuals from harm. These methods use adversarial perturbations on the input images to disrupt the outputs of the generative model.

Recent studies [29, 30, 40, 59] explored proactive defenses against diffusion models, particularly those mimicry techniques based on Latent Diffusion Models (LDM). By adding perturbations to input images, these approaches have achieved copyright protection in diffusion-based mimicry. However, existing methods fail to protect privacy in the

*Corresponding author.

audio-driven talking-head generation, which utilizes LDM to animate the given portrait. Their limitations are twofold: **1)** they cannot prevent portraits from being animated by LDM-based talking-head models with a provided audio. Although these methods may reduce the quality of the generated video, this effect alone does not ensure privacy protection. **2)** diffusion-based purification techniques can remove these protective perturbations, counteracting the quality degradation and rendering the privacy measures ineffective. Therefore, we need to generate robust adversarial perturbations that can nullify audio-driven facial movements and overcome purification techniques.

To address the above challenges with robust perturbations, we propose **Silencer**, a two-stage approach to proactively protect portrait privacy from animation by talking-head generation methods. In the first stage, we introduce a nullifying loss by disregarding audio control in the talking-head generation. Due to the lack of ground truth video, previous methods cannot be directly applied to talking-head generation. Our nullifying loss modifies the optimization objective of talking-head training to keep the portrait “silent”, as shown in Fig. 1. With the addition of adversarial noise via our nullifying loss, the generated talking videos tend to remain static, exhibiting low synchronization confidence. In the second stage, we design an anti-purification process using LDM to optimize the inverted latent feature, generating more robust perturbations. Since optimization in latent space does not have precise control over the outcomes in image space, directly applying nullifying loss to optimize the inverted latent feature would damage the adversarial portrait. Therefore, we use adversarial examples from the first stage to guide the optimization direction. To preserve the identity information, we apply a mask to the facial region halfway through the optimization process.

Overall, our main contributions are threefold:

- We introduce a benchmark for assessing proactive protection measures against privacy threats posed by advanced LDM-based talking-head generation techniques.
- We propose **Silencer**, a two-stage paradigm, to proactively protect portrait privacy with robust adversarial perturbations. First, we introduce a nullifying loss that effectively renders a portrait “silent” in the talking-head generation. Second, we develop an anti-purification strategy to enhance the robustness of these perturbations against countermeasures.
- Extensive experiments are conducted to assess the efficacy of our Silencer. Our method achieves strong privacy protection with low synchronization confidence and exhibits resistance to purification-based attacks.

2. Related Work

Audio-Driven Talking-Head Animation. Audio-driven talking-head generation has gained significant attention in

recent years with the success of generative models [1, 14, 17, 23, 31, 36, 39, 45]. Early methods [3, 7, 15, 20, 50, 54, 62, 65–67] primarily relied on Generative Adversarial Networks (GANs) [17]. However, advancements in Latent Diffusion Models (LDMs) have led to more effective techniques [5, 43, 48, 51, 54, 56, 57]. AniPortrait [54] improves visual quality and temporal consistency by projecting 3D representations as 2D landmarks in a diffusion model. In contrast, approaches like DiffTalk and Diffused Heads [43, 48] simplify the generation process by focusing on diffusion-based methods without relying on 3D models. Furthermore, EMO [51] enhances expressiveness through a direct generation framework that eliminates the need for 3D models. VASA-1 [57] performs efficient operations in the latent space for highly natural real-time generation. Hallo [56] incorporates cross-attention mechanisms and innovative audio-landmark training strategies to enhance generation quality and animation stability. In this paper, we adopt Hallo as the pre-trained talking-head model.

Adversarial Attacks in Diffusion Models. In the realm of adversarial attacks, early research introduced gradient-based methods that generate small perturbations to deceive neural network models [10, 11, 16, 18, 27, 32, 55, 63]. Building on these methods, recent studies have applied adversarial attacks to diffusion models. AdvDM [30] generates adversarial examples by optimizing latent variables during the reverse process of diffusion models. Photoguard [40] “immunizes” images by adding imperceptible perturbations that prevent diffusion models from generating realistic manipulations. Extending the ideas of AdvDM and Photoguard, Mist [29] incorporates semantic and texture loss designs to enhance cross-task transferability. Furthermore, Diff-Protect [59] introduces Score Distillation Sampling (SDS) and highlights the encoder module as the main vulnerability affecting the robustness of diffusion models.

Purification and Anti-purification. Purification methods use generative models to remove adversarial noise before classification, thereby improving resistance to adversarial manipulations [12, 19, 22, 41, 42, 46, 47, 61]. Building on this foundation, DiffPure [35] utilizes the forward and reverse processes of diffusion models to purify adversarial examples. Moreover, GridPure [64] introduces a grid-based iterative diffusion approach tailored to high-resolution images, enhancing purification effectiveness. PDM-Pure [58] uses pixel-space diffusion models as a universal purifier to mitigate adversarial noise.

To resist purification, ACA [4] maps images onto a low-dimensional latent manifold of the generative model and optimizes adversarial objectives to enable diverse content generation and control. Additionally, DiffAttack [2] introduces

an innovative, diffusion-based attack method to bypass existing purification defenses via latent feature optimization.

3. Method

3.1. Preliminary

3.1.1. Audio-driven Talking-head Generation with LDM.

Given a reference portrait p and speech audio a , talking-head generation aims to generate realistic speaking videos synchronized with speech audio. To achieve this aim with powerful text-to-image LDM models, such as Stable Diffusion [36], recent works follow a common pipeline, which utilizes ReferenceNet and audio signals to guide the animation process. ReferenceNet has the same architecture as the LDM network, which extracts appearance features from reference images for guidance. As shown in Fig. 2(b), talking-head LDM employs spatial attention to preserve intricate appearance features from the reference image. By integrating these appearance features, the model accurately captures the reference portraits, allowing for precise manipulation of facial expressions with audio inputs. Hence, during the training phase, an associated talking frame f_i is encoded into a latent representation z_0 with the encoder of Variational AutoEncoder (VAE) [13, 26]: $z_0 = \mathcal{E}(f_i)$. The diffusion process across T timesteps then transforms this latent representation to a Gaussian noise $z_T \sim \mathcal{N}(0, 1)$. The goal of the training is to progressively denoise z_T to produce a realistic talking-head frame that not only preserves the visual characteristics of the reference portrait p but also synchronizes the lip movements with the audio frame a_i . To achieve this aim, the training loss is defined by the following objective function:

$$\mathcal{L}_{l dm} = \mathbb{E}_{\mathcal{E}(f_i), p, a_i, \epsilon, t} [\|\epsilon - \epsilon_\theta(z_t, t, p, a_i)\|_2^2], \quad (1)$$

where $\epsilon \sim \mathcal{N}(0, 1)$ is a Gaussian noise, ϵ_θ represents the denoising U-Net model that processes the noisy latent variable z_t at each timestep t along with the conditional inputs, p is the reference portrait, a_i is the i -th frame of the talking-head audio.

The ability to use any person’s portrait as a reference in talking-head generation raises significant privacy concerns. To mitigate this, we propose a proactive defense mechanism centered around an open-source, advanced LDM-based talking-head generation method [56].

3.1.2. Adversarial Examples for LDM

Adversarial examples can protect images from LDM-based mimicry by finding the appropriate perturbations that can effectively cause LDM models to generate visually corrupted outputs. Previous studies have used two objective functions to exploit vulnerabilities in the diffusion model:

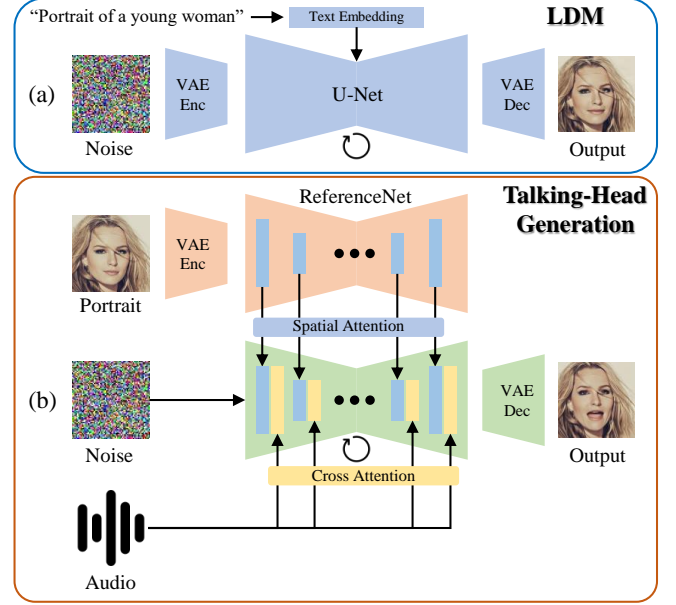


Figure 2. **LDM and LDM-based Talking-head Generation Framework.** (a) The inference process of latent diffusion models. Given random noise and text, LDM can generate a semantically coherent image through iterative denoising. (b) The talking-head generation framework. Given a portrait and audio frame, the talking-head generation model can produce a lip-sync video frame with realistic facial expressions.

- Semantic loss [30] is the training loss of LDM, which disrupts the denoising process, directing the model to produce samples that differ from the real image:

$$\mathcal{L}_S = \mathbb{E}_{t, \epsilon} \mathbb{E}_{z_t} \|\epsilon - \epsilon_\theta(z_t, t)\|_2^2 \quad (2)$$

- Texture loss [40] attacks the VAE encoder $\mathcal{E}(\cdot)$ by steering the latent representation of the input image x towards a target latent derived from another image y :

$$\mathcal{L}_T = -\|\mathcal{E}(x) - \mathcal{E}(y)\|_2^2 \quad (3)$$

The final objective \mathcal{L}_{adv} can be either semantic loss \mathcal{L}_S , texture loss \mathcal{L}_T , or both. Then PGD [34] is chosen to generate adversarial examples with projected gradient ascent:

$$x^n = \mathcal{P}_{B_\infty(x, \delta)} [x^{n-1} + \eta \text{sign} \nabla_{x^{n-1}} \mathcal{L}_{adv}(x^{n-1})] \quad (4)$$

where x^n is the adversarial example at the n -th iteration, $\mathcal{P}_{B_\infty(x, \delta)}[\cdot]$ projects the adversarial output onto the ℓ_∞ ball centered at x with budget δ , η is the step size.

3.2. Silencer

To protect portrait privacy, a straightforward approach is to directly apply semantic loss [30] to the talking-head animation task. However, this naive method presents two major

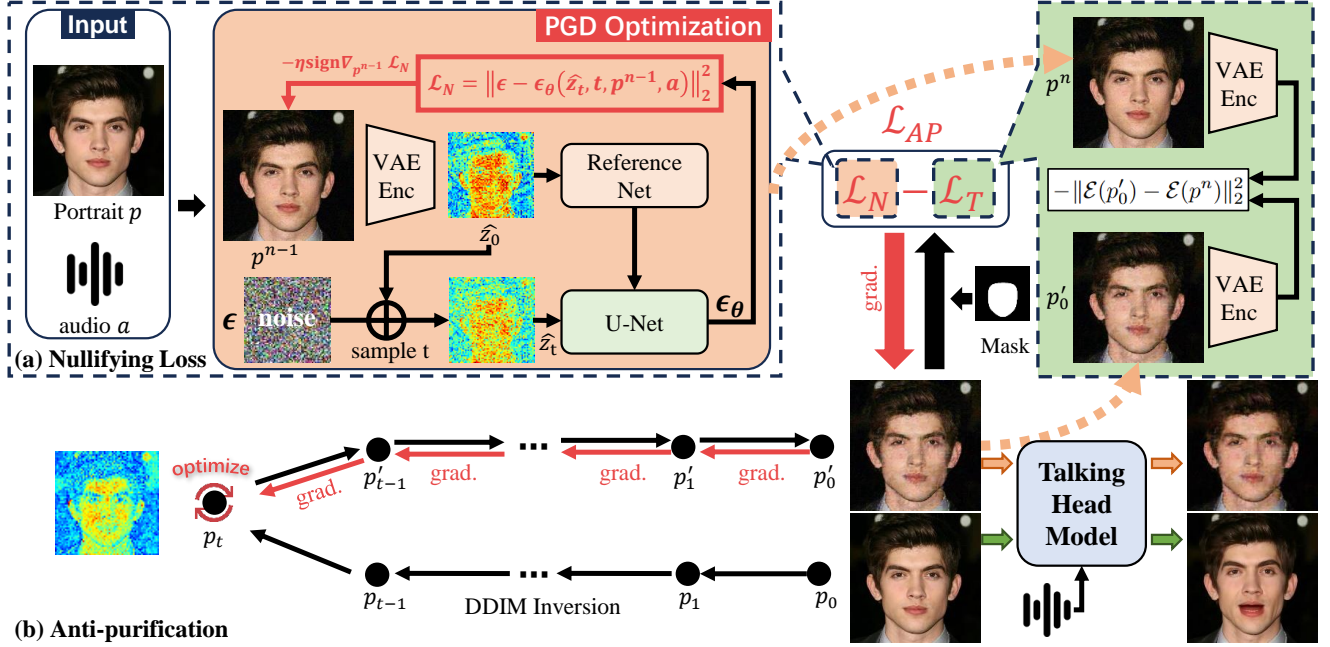


Figure 3. **Silencer Framework.** (a) In stage I, adversarial samples p^n are generated through iterative PGD optimization using our proposed nullifying loss. These samples can avoid the influence of audio in the talking-head model. (b) In stage II, our anti-purification process is employed to optimize the inverted latent features, generating more robust perturbations capable of resisting purification.

challenges: First, unlike image generation tasks, we lack ground truth frames f_i , synchronized with audio frame a_i for any arbitrary input portrait in talking-head animation. Second, we observed that noise-based perturbations introduced for privacy protection can be neutralized by purification methods. These purification methods counteract our protective measures, effectively compromising the intended privacy safeguards. In the following sections, we propose **Silencer**, a two-stage method to address these challenges.

3.2.1. Silencer-I: Nullifying Loss

To disrupt the denoising process and generate more artifacts in the edited images, semantic loss is used to optimize the perturbations by increasing or decreasing the LDM training loss. To calculate the training loss in Eq. 1, the ground truth frame f_i and the corresponding latent representation z_0 are essential. A straightforward approach is to employ existing talking-head models to generate a synchronized video frame f_i . However, this has two drawbacks. 1) Due to the time-consuming process of LDM inference, it is inefficient to generate fake ground truth under complex talking-head generation frameworks. 2) Generating fake ground truth presents a paradox: protecting portrait privacy requires it to first be compromised.

Unlike semantic loss, which requires ground truth, texture loss operates without this requirement, relying instead on a target image. Despite this advantage, texture loss does not directly affect the synchronization of the generated videos. This is primarily due to the changes of the LDM

network architecture, as shown in Fig. 2. Unlike traditional diffusion models, the LDM-based animation framework introduces conditions using ReferenceNet, which makes texture loss fail to eliminate the influence of the audio. Unless the face is fully obscured, the portrait can still be driven by audio. Hence, incorporating audio signals in the training of adversarial perturbations is crucial.

Given the limitations of existing loss functions regarding ground truth requirements and audio signal integration, we propose training adversarial perturbations that are both audio-aware and independent of ground truth. We observe that forcing the generated result to stay “silent” is an effective way to disrupt audio-visual synchronization, avoiding the need to directly attack the talking-head training process. To nullify the effect of audio signals a , we treat the reference portrait p as the ground truth of the talking-head generation. Hence, we propose a nullifying loss to disrupt the audio-visual synchronization efficiently with the following formulation:

$$\mathcal{L}_N = \mathbb{E}_t \mathbb{E}_{\mathcal{E}(p), p, a_i, \epsilon} [\|\epsilon - \epsilon_\theta(\hat{z}_t, t, p, a_i)\|_2^2], \quad (5)$$

where \hat{z}_t is the noisy latent representation at timestep t , $\mathcal{E}(p)$ is the latent representation \hat{z}_0 extracted from reference portrait p . As the reference portrait is a condition in denoising, different timestep ranges would have different attack performances. Hence, we empirically experiment on t to find the best range, as shown in Fig. 7.

Method	CelebA-HQ [25]				TalkingHead-1KH [53]			
	V-PSNR/SSIM↓	FID↑	Sync↓	M-LMD↑	V-PSNR/SSIM↓	FID↑	Sync↓	M-LMD↑
AdvDM(+) [30] [ICML23]	17.95/0.4575	78.40	5.6150	2.0425	19.09/0.4437	178.92	3.8146	1.7581
AdvDM(-) [59] [ICLR24]	16.29/0.4998	47.34	6.6670	2.1366	17.42/0.5556	52.99	5.2399	1.7244
PhotoGuard [40] [Arxiv23]	17.67/0.4763	126.09	5.8875	2.0800	18.76/0.5167	186.84	3.3784	1.9023
Mist [29] [Arxiv23]	17.80/0.4753	134.44	5.9052	2.1173	19.13/0.5241	221.58	3.0552	1.7787
SDS(+) [59] [ICLR24]	17.79/0.4569	67.23	5.8668	2.1009	19.11/0.4464	139.20	4.4844	1.6760
SDS(-) [59] [ICLR24]	16.54/0.4964	51.20	6.6743	2.0737	17.57/0.5462	57.07	5.1954	1.7301
SDTS(-) [59] [ICLR24]	17.23/0.4828	89.70	6.4003	2.1024	18.86/0.5496	139.87	3.8825	1.8579
Silencer Stage I	19.02/0.5104	124.07	4.0644	2.2008	20.61/0.5692	168.85	1.7966	1.8025
Silencer Stage II	19.01/0.5111	156.99	3.9685	2.2108	20.44/0.5718	185.87	2.0017	1.8427
Ground Truth	∞ / 1.00	0.00	6.4041	0.0000	∞ / 1.00	0.00	5.4842	0.0000

Table 1. **Quantitative Comparisons with State-of-the-art Methods on CelebA-HQ [25] and TalkingHead-1KH [53].** "↑": higher is better. "↓": lower is better. **Red**: the 1st score. **Blue**: the 2nd score.



Figure 4. **Visualization of ACA [4] and Silencer.** The result of ACA is generated by optimizing latent feature with skip gradients using our nullifying loss.

\mathcal{L}_N modifies the training target of talking-head generation from a synchronized frame to a still portrait. Then we treat \mathcal{L}_N as the adversarial loss \mathcal{L}_{adv} in Eq. 4 and optimize the reference image p with PGD for n iterations to acquire the adversarial example p^n , as shown in Fig. 3 (a). It is noted that we adopt gradient descent rather than gradient ascent to optimize the adversarial portrait:

$$p^n = \mathcal{P}_{B_\infty(p, \delta)} [p^{n-1} - \eta \text{sign } \nabla_{p^{n-1}} \mathcal{L}_N(p^{n-1})] \quad (6)$$

where p^{n-1} is the input image in n -th iteration, p^n is the output adversarial image. Not only does p^n disrupt synchronization by remaining “silent”, but it also degrades the video quality of the talking-head generation.

3.2.2. Silencer-II: Anti-purification

By optimizing a perturbation using our proposed nullifying loss, and adding it to the portrait image, we can generate an adversarial example that prevents the portrait from being driven by audio. Unfortunately, existing noise-removal or “purification” techniques can easily strip away the noise, undermining the protection effect. To address this, we need to find a more robust noise pattern that resists these purification methods, enhancing the security and effectiveness of the adversarial examples generated with our **Silencer**.

ACA [4] generates adversarial examples by applying the gradients of adversarial classification loss in the latent space inverted by DDIM [45]. While it can make natural modifications to image content, optimizing the latent vector z_T

Method	CelebA-HQ I-PSNR/SSIM↑	TalkingHead-1KH I-PSNR/SSIM↑
AdvDM(+) [30] [ICML23]	31.15/0.7605	31.32/0.7262
AdvDM(-) [59] [ICLR24]	31.02/0.7191	31.16/0.6807
PhotoGuard [40] [Arxiv23]	29.96/0.7299	30.20/0.7147
Mist [29] [Arxiv23]	30.06/0.7342	30.32/0.7190
SDS(+) [59] [ICLR24]	31.15/0.7688	31.29/0.7341
SDS(-) [59] [ICLR24]	31.26/0.7374	31.50/0.7062
SDTS(-) [59] [ICLR24]	30.42/0.7446	30.76/0.7307
Silencer Stage I	31.36/0.7475	32.34/0.7353
Silencer Stage II	27.23/0.6774	29.05/0.7590

Table 2. **Comparison on Image Quality after Protection.** Our Silencer-I achieves the best average image quality with minimal added noise while achieving protection effects.

through the skipped gradients can lead to unpredictable and undesirable changes, compromising the authenticity of the adversarial sample. These deviations are particularly pronounced in talking-head generation models, leading to significant distortions in facial identity, as shown in Fig. 4. Existing methods to address this issue, such as applying consistent constraints throughout the inversion process[2], suffer from high memory consumption and are not scalable to high-resolution portrait images.

To address the limitations of existing methods, we propose a new constrain for generating robust adversarial examples with lower computational cost. Our method, illustrated in Fig.3 (b), leverages LDM and DDIM inversion to optimize the latent representation of the image. Instead of directly adding noise, we optimize the latent features to create perturbations that are resistant to purification techniques. To ensure these perturbations are effective without significantly altering essential facial features, we utilize a constraint during the optimization process. Specifically, we extracted the VAE feature of adversarial samples generated in step I. The encoded features then serve as a constraint, during the optimization of the LDM-based adversarial example. This constrained optimization allows us to balance two objectives: maintaining crucial facial features

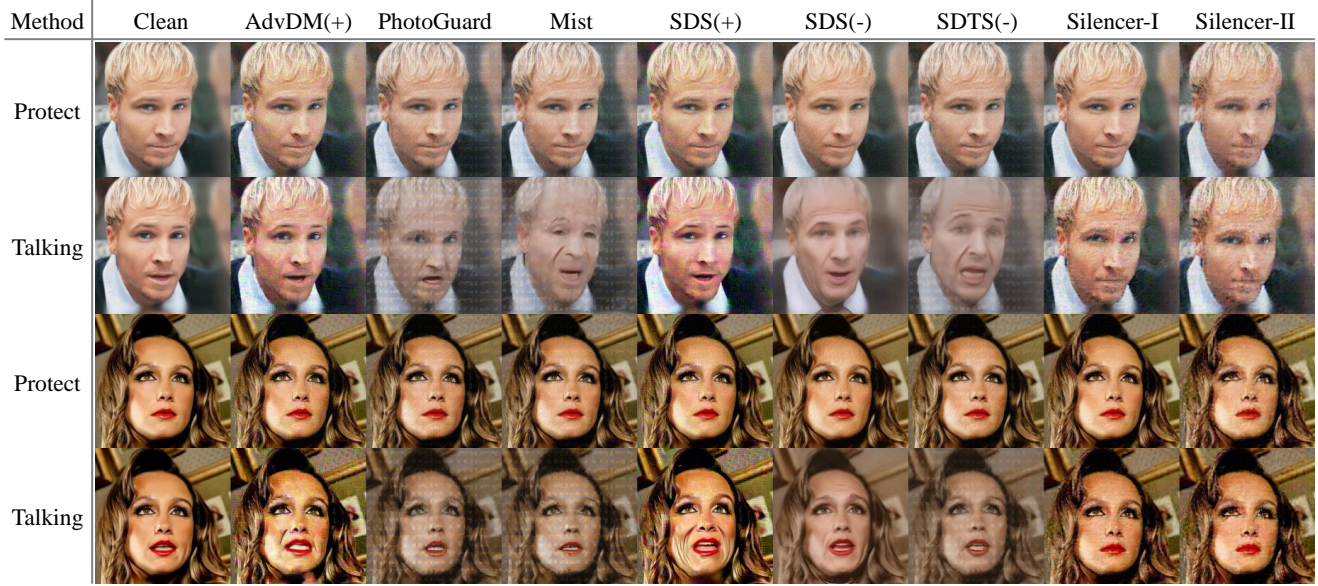


Figure 5. **Qualitative Comparison with Image Protection Methods.** We visualize the protected portraits and their frame driven by audio.

for recognition, while simultaneously maximizing the robustness of the perturbations against purification defenses. The optimization objective is formulated as follows:

$$\mathcal{L}_{AP} = \lambda_1 \mathcal{L}_N - \lambda_2 \mathcal{L}_T \quad (7)$$

$$= \lambda_1 \mathcal{L}_N + \lambda_2 \|\mathcal{E}(p'_0) - \mathcal{E}(p^n)\|_2^2 \quad (8)$$

where p'_0 is the output of the inverted diffusion model, p^n is the adversarial example generated in stage I, λ_1 and λ_2 are the corresponding coefficients. Then we use AdamW [33] to optimize the inverted latent representation p_t with \mathcal{L}_{AP} .

We observed that optimizing the entire image with \mathcal{L}_{AP} introduces considerable distortions to the facial region. LDM tends to distort the entire face in the iterative optimization process, aiming to eliminate recognizable features like the mouth and eyes. This results in a damaged face without any specific regions that could be manipulated or driven. Hence, we apply a facial mask to the optimization process that strikes a balance between face clarity and anti-purification protection. Specifically, we optimize the entire image during the initial s iterations. After this point, we restrict optimization to areas outside the masked facial region.

4. Experiments

4.1. Experimental Setup

4.1.1. Implementation Details

The videos are sampled at 25 FPS and the audio sample rate is 16KHz. The reference portraits are resized to 512×512 . We utilize Hallo [56] as the LDM-based talking-head

model with the public implementation¹. In the first stage, we adopt PGD with a budget 16/255 to train each portrait for 100 iterations, which is the same as our baselines. In the second stage, we optimize the inverted latent feature for 200 iterations with a learning rate of 0.01.

Baselines and Dataset. We compare our proposed method with four state-of-the-art privacy protection methods, including AdvDM [30], PhotoGuard [40], Mist [29] and SDS [59]. To evaluate the performance of protection baselines, we select 50 images from the CelebA-HQ [25] dataset as the reference images and one audio as the driving signal. To create a more realistic scenario, we utilize CLIP-IQA [52] to select 50 high-quality video clips, each with a unique identity and associated speech audio, from the widely used TalkingHead-1KH dataset [53].

4.1.2. Metrics

We assess the quality of synthesized emotional videos with the following metrics:

Image quality. We utilize Peak Signal-to-Noise Ratio (PSNR), Structural Similarity Index Measure (SSIM), and Fréchet Inception Distance score (FID) [21] to measure the image quality of synthesized videos. The video metrics, V-PSNR/SSIM, measure PSNR/SSIM specifically on facial regions. In contrast, the image metrics, I-PSNR/SSIM, calculate PSNR and SSIM across the entire image by comparing the original image with the adversarial image. The Fréchet Inception Distance (FID) is a common metric for measuring the fidelity of synthesized videos. It quantifies

¹<https://github.com/fudan-generative-vision/hallo>

Method		Protected I-PSNR/FID	JPEG [42] I-PSNR↓/FID↑	AdvClean I-PSNR↓/FID↑	DiffPure [35] I-PSNR↓/FID↑	GrIDPure [64] I-PSNR↓/FID↑
AdvDM(+) [30]	[ICML23]	31.15/86.58	31.35/62.09	33.65/49.36	28.78/44.83	27.81/38.55
AdvDM(-) [59]	[ICLR24]	31.02/66.73	31.96/36.97	33.29/40.17	29.11/42.17	27.86/25.48
PhotoGuard [40]	[Arxiv23]	29.96/153.50	30.37/96.98	31.37/109.87	28.36/48.43	26.32/50.04
Mist [29]	[Arxiv23]	30.06/156.42	30.47/ 99.72	31.51/108.92	28.40/44.14	26.35/49.88
SDS(+) [59]	[ICLR24]	31.15/86.41	31.30/60.47	33.58/44.80	28.72/44.23	27.81/38.29
SDS(-) [59]	[ICLR24]	31.26/70.93	32.24/40.69	33.31/48.07	29.10/39.92	27.89/25.90
SDTS(-) [59]	[ICLR24]	30.42/112.43	30.97/72.90	31.89/82.19	28.53/47.97	26.63/39.90
Silencer	Stage I	31.36/135.77	33.38/55.94	35.03/61.38	29.26/38.93	28.16/20.85
Silencer	Stage II	27.23/175.21	27.41/159.34	27.95/135.30	27.26/87.22	25.72/144.89

Table 3. **Purification Experiments on CelebA-HQ [25]**. The “Protected” is the metrics calculated with protected portraits for reference. Others are calculated with purified portraits. “↑”: higher is better. “↓”: lower is better. **Red**: the 1st score. **Blue**: the 2nd score.

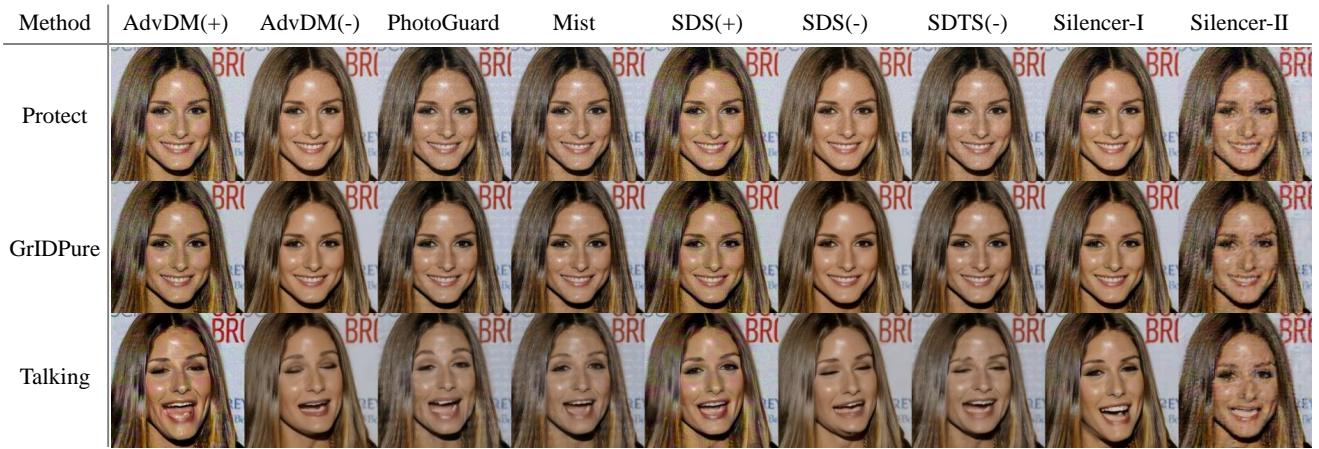


Figure 6. **Visual Comparison in Anti-purification**. The third row is the animated talking frames with the portraits after GrIDPure [64].

the distribution distance between videos generated using original and protected portraits.

Audio-visual synchronization. We evaluate the audio-visual synchronization of the synthesized videos using SyncNet’s confidence score [6, 15]. In addition, the distance between the landmarks of the mouth (M-LMD) [3] is used to indicate speech content consistency.

4.2. Privacy Protection

We first compare the effectiveness of our Silencer in privacy protection with other state-of-the-art methods. We randomly selected an audio from TalkingHead-1KH dataset for training all adversarial example and tested the talking-head model with other audios. In CelebA-HQ, all tests used the same audio clip, while in TalkingHead-1KH, each face was tested with its original audio. We treat videos generated by Hallo using the portraits without protection as the ground truth for comparison.

Table 1 shows that our method achieves the best synchronization protection, with a score of 3.9685 on CelebA-HQ and 2.0017 on TalkingHead-1KH. In stage I of Silencer,

our nullifying loss effectively frees reference portraits from audio control during talking-head generation. In stage II, our Silencer continues to yield strong results, further validating the effectiveness of our method. In terms of video quality, our method can only achieve comparable results in the video FID. This is primarily due to our nullifying loss, which aims to ensure the reference portrait remains largely unchanged during the diffusion process. As a result, our method has less impact on the generated video quality compared to others. Table 2 shows that Silencer-I achieves the highest I-PSNR, indicating minimal degradation of the reference portrait’s realism. Furthermore, the qualitative comparison in Fig. 5 reveals that, unlike methods that significantly alter facial appearance, our approach preserves visual consistency while “silencing” the talking head. These results underscore the effectiveness of our method in achieving privacy protection from audio control.

4.3. Anti-Purification Experiments

To demonstrate the effectiveness of our methods in resisting purification, we conduct purification on the protected

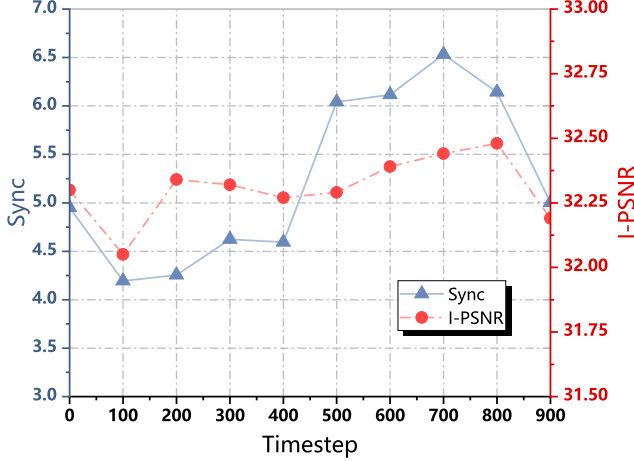


Figure 7. Ablation Study on Timestep Ranges in Silencer-I.

portraits. We select the following advanced purification methods to attack: JPEG [42], AdvClean, Diff-Pure [35] and GrIDPure [64]. We evaluate anti-purification effectiveness using I-PSNR, comparing original and purified images, and FID for talking-head videos, comparing ground truth to videos generated with purified portraits from a CelebA-HQ subset. Table 3 shows Silencer-II achieves the best anti-purification performance, with the lowest I-PSNR and highest FID. This is because adversarial noises, generated by Silencer-I and other methods, are optimized in the image space with PGD [34] and can be easily purified. In contrast, Silencer-II optimizes perturbations within the LDM’s inverted latent space, resulting in fundamentally different and more robust perturbations. Fig. 6 visually demonstrates this efficacy. Although our generated perturbations resist complete removal, their structure is altered by purification, preventing a perfectly “silent” portrait. Achieving a completely robust perturbation that results in a “silent” portrait even after purification remains a challenge. We will explore more robust solutions in future work.

4.4. Ablation Study

Ablation Study on Timestep Ranges in Silencer-I.

Since the reference portrait serves as a condition in the denoising process, adjusting the timestep range results in varying levels of attack effectiveness. To identify the optimal timestep ranges, we divided the total of 1000 timesteps into ten equal segments, sampling 100 timesteps from each segment for training. We trained and evaluated our model on the subset of CelebA-HQ, with the results illustrated in Fig. 7. Our findings indicate that timesteps within the [200, 300] range achieve a desirable balance: they provide effective privacy protection, with a sync confidence of 4.2556, while maintaining minimal noise, with an I-PSNR of 32.34. Based on these results, we selected the [200, 300] range for

Ablation	SDTS(-)	S-I	S-II (A)	S-II (B)
\mathcal{L}_N		✓	✓	✓
Anti-purify			✓	✓
Mask				✓
I-SSIM↑	0.7446	0.7475	0.6561	0.6774
FID↑	89.70	124.07	167.40	156.99
Sync↓	6.4003	4.0644	3.4339	3.9685
M-LMD↑	2.1024	2.2008	2.3607	2.2108

Table 4. Ablation Study of Each Component. Each component contributes to improving privacy protection, thus verifying its effectiveness.

timestep sampling in training Silencer-I.

Ablation Study on Each Component. We conduct an ablation study to evaluate the impact of each component of our Silencer using the CelebA-HQ dataset. As shown in Table 4, the introduction of our nullifying loss leads to a significant reduction in synchronization confidence compared to previous methods. Additionally, the anti-purification process remains the low synchronization, providing protection against talking-head manipulation. However, this comes at the cost of reduced visual quality. To mitigate this, we optimize the adversarial perturbation with a face mask, which preserves facial structure while achieving effective privacy protection. More experiments can be found in our supplementary material.

5. Conclusion

In this paper, we introduce **Silencer**, a two-stage approach to proactively protect portrait privacy from unauthorized animation in audio-driven talking-head generation. This approach addresses the limitations of prior methods that cannot effectively mitigate talking animation and resist purification. The first stage employs a novel nullifying loss to decouple facial movements from audio input, significantly reducing the synchronization of generated talking-head videos. Building upon this, the second stage enhances robustness through an anti-purification process. This process optimizes perturbations within the inverted latent space of an LDM, guided by adversarial examples from the first stage to ensure targeted and effective protection. A strategically applied mask preserves facial integrity during this optimization. Extensive experiments demonstrate Silencer’s superior performance in both preventing unauthorized animation and resisting purification, confirming its effectiveness in protecting portrait privacy. This work establishes a new benchmark for proactive privacy protection in LDM-based talking-head generation and we anticipate it will stimulate further research and development in this critical area.

Acknowledgments

This work was supported in part by the Key R&D Program of China (2021ZD0112801), the Key Program of National Natural Science Foundation of China (62436007) and the Natural Science Foundation of Zhejiang Province (LDT23F02023F02).

References

- [1] Yihan Cao, Siyu Li, Yixin Liu, Zhiling Yan, Yutong Dai, Philip S Yu, and Lichao Sun. A comprehensive survey of ai-generated content (aigc): A history of generative ai from gan to chatgpt. *arXiv preprint arXiv:2303.04226*, 2023. 2
- [2] Jianqi Chen, Hao Chen, Keyan Chen, Yilan Zhang, Zhengxia Zou, and Zhenwei Shi. Diffusion models for imperceptible and transferable adversarial attack. *IEEE Transactions on Pattern Analysis and Machine Intelligence*, pages 1–17, 2024. 2, 5
- [3] Lele Chen, Ross K Maddox, Zhiyao Duan, and Chenliang Xu. Hierarchical cross-modal talking face generation with dynamic pixel-wise loss. In *Proceedings of the IEEE/CVF Conference on Computer Vision and Pattern Recognition*, pages 7832–7841, 2019. 1, 2, 7
- [4] Zhaoyu Chen, Bo Li, Shuang Wu, Kaixun Jiang, Shouhong Ding, and Wenqiang Zhang. Content-based unrestricted adversarial attack. In *Thirty-seventh Conference on Neural Information Processing Systems*, 2023. 2, 5
- [5] Zhiyuan Chen, Jiajiong Cao, Zhiquan Chen, Yuming Li, and Chenguang Ma. Echomimic: Lifelike audio-driven portrait animations through editable landmark conditioning, 2024. 1, 2, 12
- [6] Joon Son Chung and Andrew Zisserman. Out of time: automated lip sync in the wild. In *Asian conference on computer vision*, pages 251–263. Springer, 2016. 7
- [7] Joon Son Chung, Amir Jamaludin, and Andrew Zisserman. You said that? *BMVC*, 2017. 2
- [8] Jiahao Cui, Hui Li, Yao Yao, Hao Zhu, Hanlin Shang, Kaihui Cheng, Hang Zhou, Siyu Zhu, and Jingdong Wang. Hallo2: Long-duration and high-resolution audio-driven portrait image animation. *arXiv preprint arXiv:2410.07718*, 2024. 1, 12
- [9] Hao Dang, Feng Liu, Joel Stehouwer, Xiaoming Liu, and Anil K Jain. On the detection of digital face manipulation. In *Proceedings of the IEEE/CVF Conference on Computer Vision and Pattern Recognition*, pages 5781–5790, 2020. 1
- [10] Yinpeng Dong, Fangzhou Liao, Tianyu Pang, Hang Su, Jun Zhu, Xiaolin Hu, and Jianguo Li. Boosting adversarial attacks with momentum. In *Proceedings of the IEEE conference on computer vision and pattern recognition*, pages 9185–9193, 2018. 2
- [11] Yinpeng Dong, Tianyu Pang, Hang Su, and Jun Zhu. Evading defenses to transferable adversarial examples by translation-invariant attacks. In *Proceedings of the IEEE/CVF conference on computer vision and pattern recognition*, pages 4312–4321, 2019. 2
- [12] Yilun Du and Igor Mordatch. Implicit generation and modeling with energy based models. In *Advances in Neural Information Processing Systems*. Curran Associates, Inc., 2019. 2
- [13] Patrick Esser, Robin Rombach, and Bjorn Ommer. Taming transformers for high-resolution image synthesis. In *Proceedings of the IEEE/CVF conference on computer vision and pattern recognition*, pages 12873–12883, 2021. 3
- [14] Sheng Fan, Rui Liu, Wenguan Wang, and Yi Yang. Navigation instruction generation with bev perception and large language models. In *ECCV*, 2024. 2
- [15] Yuan Gan, Zongxin Yang, Xihang Yue, Lingyun Sun, and Yi Yang. Efficient emotional adaptation for audio-driven talking-head generation. In *Proceedings of the IEEE/CVF International Conference on Computer Vision*, pages 22634–22645, 2023. 1, 2, 7
- [16] Lianli Gao, Qilong Zhang, Jingkuan Song, Xianglong Liu, and Heng Tao Shen. Patch-wise attack for fooling deep neural network. In *Computer Vision—ECCV 2020: 16th European Conference, Glasgow, UK, August 23–28, 2020, Proceedings, Part XXVIII 16*, pages 307–322. Springer, 2020. 2
- [17] Ian J Goodfellow, Jean Pouget-Abadie, Mehdi Mirza, Bing Xu, David Warde-Farley, Sherjil Ozair, Aaron Courville, and Yoshua Bengio. Generative adversarial nets. *Advances in neural information processing systems*, 27, 2014. 2
- [18] Ian J Goodfellow, Jonathon Shlens, and Christian Szegedy. Explaining and harnessing adversarial examples. *arXiv preprint arXiv:1412.6572*, 2014. 2
- [19] Will Grathwohl, Kuan-Chieh Wang, Jörn-Henrik Jacobsen, David Duvenaud, Mohammad Norouzi, and Kevin Swersky. Your classifier is secretly an energy based model and you should treat it like one. *arXiv preprint arXiv:1912.03263*, 2019. 2
- [20] Yudong Guo, Keyu Chen, Sen Liang, YongJin Liu, Hujun Bao, and Juyong Zhang. Ad-nerf: Audio driven neural radiance fields for talking head synthesis. In *Proceedings of the IEEE/CVF International Conference on Computer Vision*, pages 5784–5794, 2021. 1, 2
- [21] Martin Heusel, Hubert Ramsauer, Thomas Unterthiner, Bernhard Nessler, and Sepp Hochreiter. Gans trained by a two time-scale update rule converge to a local nash equilibrium. *Advances in neural information processing systems*, 30, 2017. 6
- [22] Mitch Hill, Jonathan Mitchell, and Song-Chun Zhu. Stochastic security: Adversarial defense using long-run dynamics of energy-based models. *arXiv preprint arXiv:2005.13525*, 2020. 2
- [23] Jonathan Ho, Ajay Jain, and Pieter Abbeel. Denoising diffusion probabilistic models. *Advances in neural information processing systems*, 33:6840–6851, 2020. 2
- [24] Li Hu. Animate anyone: Consistent and controllable image-to-video synthesis for character animation. In *Proceedings of the IEEE/CVF Conference on Computer Vision and Pattern Recognition*, pages 8153–8163, 2024. 1
- [25] Tero Karras, Timo Aila, Samuli Laine, and Jaakko Lehtinen. Progressive growing of gans for improved quality, stability, and variation. In *International Conference on Learning Representations*, 2018. 5, 6, 7, 14

- [26] Diederik P. Kingma and Max Welling. Auto-encoding variational bayes. In *ICLR*, 2014. 3
- [27] Alexey Kurakin, Ian J Goodfellow, and Samy Bengio. Adversarial examples in the physical world. In *Artificial intelligence safety and security*, pages 99–112. Chapman and Hall/CRC, 2018. 2
- [28] Zheng Li, Ning Yu, Ahmed Salem, Michael Backes, Mario Fritz, and Yang Zhang. Uganable: Defending against gan-based face manipulation. In *32nd USENIX Security Symposium (USENIX Security 23)*, pages 7213–7230, 2023. 1
- [29] Chumeng Liang and Xiaoyu Wu. Mist: Towards improved adversarial examples for diffusion models. *arXiv preprint arXiv:2305.12683*, 2023. 1, 2, 5, 6, 7
- [30] Chumeng Liang, Xiaoyu Wu, Yang Hua, Jiaru Zhang, Yiming Xue, Tao Song, Zhengui Xue, Ruhui Ma, and Haibing Guan. Adversarial example does good: Preventing painting imitation from diffusion models via adversarial examples. In *International Conference on Machine Learning*, pages 20763–20786. PMLR, 2023. 1, 2, 3, 5, 6, 7
- [31] Yaron Lipman, Ricky TQ Chen, Heli Ben-Hamu, Maximilian Nickel, and Matt Le. Flow matching for generative modeling. *arXiv preprint arXiv:2210.02747*, 2022. 2
- [32] Yuyang Long, Qilong Zhang, Boheng Zeng, Lianli Gao, Xianglong Liu, Jian Zhang, and Jingkuan Song. Frequency domain model augmentation for adversarial attack. In *European conference on computer vision*, pages 549–566. Springer, 2022. 2
- [33] I Loshchilov. Decoupled weight decay regularization. *arXiv preprint arXiv:1711.05101*, 2017. 6
- [34] Aleksander Madry. Towards deep learning models resistant to adversarial attacks. *arXiv preprint arXiv:1706.06083*, 2017. 3, 8
- [35] Weili Nie, Brandon Guo, Yujia Huang, Chaowei Xiao, Arash Vahdat, and Anima Anandkumar. Diffusion models for adversarial purification. *arXiv preprint arXiv:2205.07460*, 2022. 2, 7, 8, 12
- [36] Robin Rombach, Andreas Blattmann, Dominik Lorenz, Patrick Esser, and Björn Ommer. High-resolution image synthesis with latent diffusion models. In *Proceedings of the IEEE/CVF conference on computer vision and pattern recognition*, pages 10684–10695, 2022. 1, 2, 3
- [37] Andreas Rossler, Davide Cozzolino, Luisa Verdoliva, Christian Riess, Justus Thies, and Matthias Nießner. Faceforensics++: Learning to detect manipulated facial images. In *Proceedings of the IEEE/CVF international conference on computer vision*, pages 1–11, 2019. 1
- [38] Nataniel Ruiz, Sarah Adel Bargal, and Stan Sclaroff. Disrupting deepfakes: Adversarial attacks against conditional image translation networks and facial manipulation systems. In *Computer Vision—ECCV 2020 Workshops: Glasgow, UK, August 23–28, 2020, Proceedings, Part IV 16*, pages 236–251. Springer, 2020. 1
- [39] Nataniel Ruiz, Yuanzhen Li, Varun Jampani, Yael Pritch, Michael Rubinstein, and Kfir Aberman. Dreambooth: Fine tuning text-to-image diffusion models for subject-driven generation. In *Proceedings of the IEEE/CVF conference on computer vision and pattern recognition*, pages 22500–22510, 2023. 2
- [40] Hadi Salman, Alaa Khaddaj, Guillaume Leclerc, Andrew Ilyas, and Aleksander Madry. Raising the cost of malicious ai-powered image editing. *arXiv preprint arXiv:2302.06588*, 2023. 1, 2, 3, 5, 6, 7
- [41] P Samangouei. Defense-gan: protecting classifiers against adversarial attacks using generative models. *arXiv preprint arXiv:1805.06605*, 2018. 2
- [42] Pedro Sandoval-Segura, Jonas Geiping, and Tom Goldstein. Jpeg compressed images can bypass protections against ai editing. *arXiv preprint arXiv:2304.02234*, 2023. 2, 7, 8
- [43] Shuai Shen, Wenliang Zhao, Zibin Meng, Wanhua Li, Zheng Zhu, Jie Zhou, and Jiwen Lu. Difftalk: Crafting diffusion models for generalized audio-driven portraits animation. In *CVPR*, 2023. 2
- [44] Kaede Shiohara and Toshihiko Yamasaki. Detecting deepfakes with self-blended images. In *Proceedings of the IEEE/CVF Conference on Computer Vision and Pattern Recognition*, pages 18720–18729, 2022. 1
- [45] Jiaming Song, Chenlin Meng, and Stefano Ermon. Denoising diffusion implicit models. *arXiv preprint arXiv:2010.02502*, 2020. 2, 5
- [46] Yang Song and Stefano Ermon. Generative modeling by estimating gradients of the data distribution. *Advances in neural information processing systems*, 32, 2019. 2
- [47] Yang Song, Taesup Kim, Sebastian Nowozin, Stefano Ermon, and Nate Kushman. Pixeldefend: Leveraging generative models to understand and defend against adversarial examples. *arXiv preprint arXiv:1710.10766*, 2017. 2
- [48] Michał Stypułkowski, Konstantinos Vougioukas, Sen He, Maciej Zięba, Stavros Petridis, and Maja Pantic. Diffused heads: Diffusion models beat gans on talking-face generation. In *Proceedings of the IEEE/CVF Winter Conference on Applications of Computer Vision*, pages 5091–5100, 2024. 2
- [49] Chuangchuang Tan, Yao Zhao, Shikui Wei, Guanghua Gu, Ping Liu, and Yunchao Wei. Rethinking the up-sampling operations in cnn-based generative network for generalizable deepfake detection. In *Proceedings of the IEEE/CVF Conference on Computer Vision and Pattern Recognition*, pages 28130–28139, 2024. 1
- [50] Shuai Tan, Bin Ji, Mengxiao Bi, and Ye Pan. Edtalk: Efficient disentanglement for emotional talking head synthesis. In *European Conference on Computer Vision*, pages 398–416. Springer, 2024. 1, 2
- [51] Linrui Tian, Qi Wang, Bang Zhang, and Liefeng Bo. Emo: Emote portrait alive-generating expressive portrait videos with audio2video diffusion model under weak conditions. *arXiv preprint arXiv:2402.17485*, 2024. 2
- [52] Jianyi Wang, Kelvin CK Chan, and Chen Change Loy. Exploring clip for assessing the look and feel of images. In *Proceedings of the AAAI Conference on Artificial Intelligence*, pages 2555–2563, 2023. 6
- [53] Ting-Chun Wang, Arun Mallya, and Ming-Yu Liu. One-shot free-view neural talking-head synthesis for video conferencing. In *CVPR*, 2021. 5, 6, 14
- [54] Huawei Wei, Zejun Yang, and Zhisheng Wang. Aniportrait: Audio-driven synthesis of photorealistic portrait animations, 2024. 1, 2

- [55] Cihang Xie, Zhishuai Zhang, Yuyin Zhou, Song Bai, Jianyu Wang, Zhou Ren, and Alan L Yuille. Improving transferability of adversarial examples with input diversity. In *Proceedings of the IEEE/CVF conference on computer vision and pattern recognition*, pages 2730–2739, 2019. [2](#)
- [56] Mingwang Xu, Hui Li, Qingkun Su, Hanlin Shang, Liwei Zhang, Ce Liu, Jingdong Wang, Luc Van Gool, Yao Yao, and Siyu Zhu. Hallo: Hierarchical audio-driven visual synthesis for portrait image animation. *arXiv preprint arXiv:2406.08801*, 2024. [2](#), [3](#), [6](#)
- [57] Sicheng Xu, Guojun Chen, Yu-Xiao Guo, Jiaolong Yang, Chong Li, Zhenyu Zang, Yizhong Zhang, Xin Tong, and Baining Guo. Vasa-1: Lifelike audio-driven talking faces generated in real time. *arXiv preprint arXiv:2404.10667*, 2024. [1](#), [2](#)
- [58] Haotian Xue and Yongxin Chen. Pixel is a barrier: Diffusion models are more adversarially robust than we think. *arXiv preprint arXiv:2404.13320*, 2024. [2](#)
- [59] Haotian Xue, Chumeng Liang, Xiaoyu Wu, and Yongxin Chen. Toward effective protection against diffusion-based mimicry through score distillation. In *The Twelfth International Conference on Learning Representations*, 2023. [1](#), [2](#), [5](#), [6](#), [7](#)
- [60] Zhiyuan Yan, Yong Zhang, Yanbo Fan, and Baoyuan Wu. Ucf: Uncovering common features for generalizable deepfake detection. In *Proceedings of the IEEE/CVF International Conference on Computer Vision*, pages 22412–22423, 2023. [1](#)
- [61] Jongmin Yoon, Sung Ju Hwang, and Juho Lee. Adversarial purification with score-based generative models. In *International Conference on Machine Learning*, pages 12062–12072. PMLR, 2021. [2](#)
- [62] Wenxuan Zhang, Xiaodong Cun, Xuan Wang, Yong Zhang, Xi Shen, Yu Guo, Ying Shan, and Fei Wang. Sadtalker: Learning realistic 3d motion coefficients for stylized audio-driven single image talking face animation. In *Proceedings of the IEEE/CVF Conference on Computer Vision and Pattern Recognition*, pages 8652–8661, 2023. [1](#), [2](#)
- [63] Zhengyu Zhao, Zhuoran Liu, and Martha Larson. Towards large yet imperceptible adversarial image perturbations with perceptual color distance. In *Proceedings of the IEEE/CVF conference on computer vision and pattern recognition*, pages 1039–1048, 2020. [2](#)
- [64] Zhengyue Zhao, Jinhao Duan, Kaidi Xu, Chenan Wang, Rui Zhang, Zidong Du, Qi Guo, and Xing Hu. Can protective perturbation safeguard personal data from being exploited by stable diffusion? In *Proceedings of the IEEE/CVF Conference on Computer Vision and Pattern Recognition*, pages 24398–24407, 2024. [2](#), [7](#), [8](#), [12](#)
- [65] Hang Zhou, Yu Liu, Ziwei Liu, Ping Luo, and Xiaogang Wang. Talking face generation by adversarially disentangled audio-visual representation. In *Proceedings of the AAAI Conference on Artificial Intelligence*, pages 9299–9306, 2019. [2](#)
- [66] Hang Zhou, Yasheng Sun, Wayne Wu, Chen Change Loy, Xiaogang Wang, and Ziwei Liu. Pose-controllable talking face generation by implicitly modularized audio-visual representation. In *Proceedings of the IEEE/CVF conference on computer vision and pattern recognition*, pages 4176–4186, 2021. [1](#)
- [67] Yang Zhou, Xintong Han, Eli Shechtman, Jose Echevarria, Evangelos Kalogerakis, and Dingzeyu Li. Makelttalk: speaker-aware talking-head animation. *ACM Transactions on Graphics (TOG)*, 39(6):1–15, 2020. [1](#), [2](#)

A. More Experiments

A.1. More Implementation Details

The resolution of our input portrait is 512×512 . The audio used for training in our experiment is a four-second clip. For testing on CelebA-HQ, the audio length is seven seconds. In the case of TalkingHead-1KH, the audio length varies between three and seven seconds. In our experiment, the DDIM inversion step is set to 20. Due to the limitation of GPU memory, we optimize only the inverted latent feature from the final step. All experiments can be conducted using a single NVIDIA A40 GPU.

A.2. Evaluating the Transferability of Silencer

To evaluate the transferability of **Silencer (S-I and S-II)**, we performed a cross-model evaluation. Adversarial noise was optimized on the Hallo model and subsequently tested on other LDM-based talking-head generation models. Specifically, we randomly selected 20 portraits from the TalkingHead-1KH dataset and generated talking-head videos using the publicly available EchoMimic [5] and Hallo2 [8]. As shown in Table 5, the synchronization values of the generated videos demonstrate that Silencer maintains a significant adversarial effect even when applied to models different from the one used for optimization. Although **Silencer** is designed as a white-box attack, these results highlight its notable generalization capability across various LDM-based talking-head models. This cross-model robustness suggests the potential for broader applicability and further validates the effectiveness of our method. A likely explanation for the observed cross-model effectiveness of Silencer is a combination of factors. First, these LDM-based talking-head models share similar architectural designs. Second, and perhaps more crucially, they are all fine-tuned upon Stable Diffusion. This common foundation could introduce common weaknesses or biases that Silencer is able to exploit, even across different models.

A.3. Efficiency Analysis

We evaluated the computational efficiency on an NVIDIA A40 GPU. The results, shown in Table 6, demonstrate a significant difference in Silencer-I and Silencer-II. Silencer-I exhibits superior efficiency, requiring considerably less computational time compared to Silencer-II. This difference in efficiency stems primarily from the architectural design of Silencer-II. Unlike Silencer-I, Silencer-II incorporates an optimization step within the latent space of an additional LDM. This additional optimization process introduces a substantial computational overhead, increasing the overall time required for Silencer-II to generate adversarial examples. While this optimization contributes to more robust perturbations, it comes at the cost of reduced computational efficiency. Silencer-I, by contrast, avoids this ex-

Method	GT	AdvDM(+)	Mist	SDST(-)	S-I	S-II
EchoMimic [5]	4.0365	1.8252	1.7839	2.2228	1.4601	0.9973
Hallo2 [8]	5.6661	3.2136	3.0679	3.9238	1.5952	2.0783

Table 5. **Evaluating the Transferability of Silencer.** Synchronization scores demonstrating cross-model transferability of Silencer (S-I and S-II). Videos were generated by EchoMimic [5] and Hallo2 [8] using original (GT) and adversarial inputs. Lower scores signify greater disruption. Despite being optimized on Hallo, Silencer significantly impacts both models.

	AdvDM(+)	PhotoGuard	Mist	SDS(-)	SDST(-)	S-I	S-II
time	59	34	59	22	40	64	241

Table 6. **Efficiency Analysis.** Average time (seconds/image) required for different protection methods.

DiffPure timesteps	50	100	150
Silencer-I	30.65/0.2606	29.26/0.2540	28.13/0.2691
Silencer-II	27.80/0.4057	27.26/0.3909	26.82/0.3504

Table 7. **Ablation on Timesteps of DiffPure [35].** We present I-PSNR/LPIPS scores for Silencer-I and Silencer-II after applying DiffPure with varying timesteps. Red values highlight greater robustness.

GrIDPure timesteps	5	10	15
Silencer-I	28.35/0.1672	28.16/0.1698	27.93/0.2016
Silencer-II	25.81/0.3451	25.72/0.3511	25.59/0.3610

Table 8. **Ablation on Timesteps of GrIDPure [64].** We present I-PSNR/LPIPS scores for Silencer-I and Silencer-II after applying GrIDPure purification. GrIDPure was run for 20 iterations with initial timesteps of 5, 10, and 15. Red values highlight greater robustness.

tra optimization step, leading to a more streamlined and faster process. While Silencer-I takes 64 seconds per image, its runtime is comparable to other methods like AdvDM(+) and Mist (59 seconds). This makes Silencer-I a more practical choice in scenarios where computational resources are limited or where rapid generation of adversarial examples is critical. Notably, SDS(-) demonstrate significantly faster runtimes, due to skipping the UNet portion of the gradient calculation. However, whether such an optimization can be effectively and reliably applied within an LDM-based talking-head network to improve efficiency remains an open challenge for future research.

	DiffAudio	SameAudio
Silencer-II	3.9685	2.4926
Ground Truth	6.4041	5.7509

Table 9. **Impact of Audio Consistency on Silencer-II while Training and Testing with CelebA-HQ.** "DiffAudio" denotes using different audio for training and testing, while "SameAudio" uses the same audio. Lower Sync value is better.

l_{inf}	V-PSNR/SSIM↓	FID↑	Sync↓	M-LMD↑
8/255	19.59/0.5768	78.78	4.8368	2.0444
16/255	19.02/0.5104	124.07	4.0644	2.2008

Table 10. **Ablation Study of l_{inf} Perturbation Budgets in Silencer-I on CelebA-HQ.**

Inverted Timesteps	V-PSNR/SSIM↓	FID↑	Sync↓	M-LMD↑
the last one	19.01/0.5111	156.99	3.9685	2.2108
the last two	19.30/0.5402	111.99	4.4579	2.1731

Table 11. **Ablation Study of Inverted Timesteps in Silencer-II on CelebA-HQ.**

A.4. More Ablation Study

Ablation Study on Timesteps in Purification Methods. Our anti-purification experiments are conducted using the publicly available implementation². For DiffPure, we set the diffusion timestep to 100, while for GrIDPure, we use a timestep of 10 with 20 iterations. We conduct the ablation experiments on different settings of diffusion-based purification. Table 7 and Table 8 illustrate the effectiveness of Silencer-I and Silencer-II against image purification techniques, specifically DiffPure and GrIDPure, across different timesteps. The tables compare I-PSNR and LPIPS scores for images processed by both Silencer versions. While larger timesteps in these purification methods improve the smoothness of the resulting images, they fail to completely remove the perturbations introduced by Silencer-II. This highlights the robustness of our approach.

Ablation Study on Audio and Portrait in the Training and Testing of CelebA-HQ. For audio, We investigated the effect of using the same versus different audio inputs during the training and testing phases. This tests whether Silencer is overly sensitive to specific audio characteristics or if it can generalize to unseen audio. As shown in Table 9, both scenarios resulted in a reduction of the synchronization value compared to the ground truth. The decrease in

²<https://github.com/zhengyuezhao/gridpure>

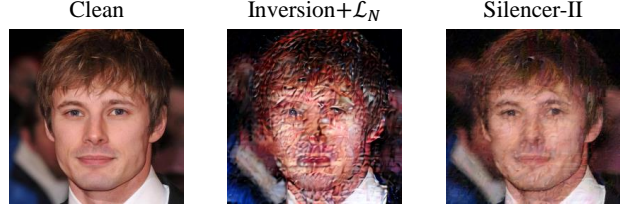


Figure 8. **Ablation Study on \mathcal{L}_T in Silencer-II.** Without the assistance of \mathcal{L}_T , the generated perturbation becomes highly noticeable, significantly compromising the facial identity.

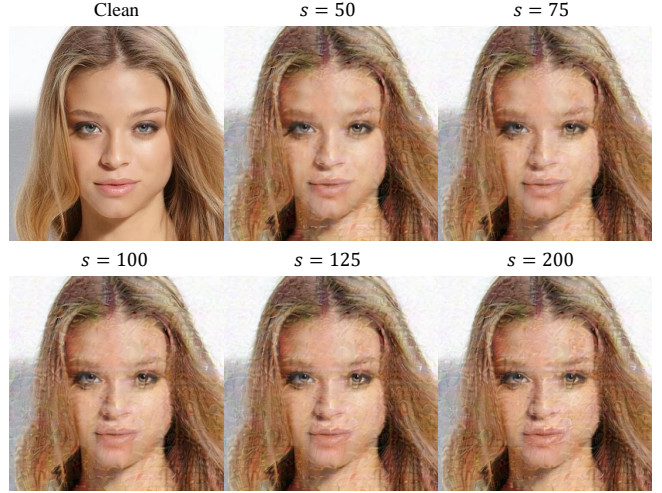


Figure 9. **Visualization Results with Different Iteration s .** The quality of the portrait decreases with the growth of s .

s	50	75	100	125	200
I-SSIM↑	0.7125	0.6998	0.6918	0.6844	0.6704
FID↑	136.88	166.10	173.18	171.08	193.46
Sync↓	5.5725	5.0413	4.0602	4.1832	4.0791
M-LMD↑	1.8559	2.1371	2.2053	2.3748	2.3563

Table 12. **Ablation Study on the Initial Iteration s without Mask.** Larger iterations without the face mask lead to better protection performance with lower image quality.

synchronization demonstrates that Silencer effectively disrupts synchronization regardless of whether the audio input is consistent between training and testing. This finding highlights the robustness of the Silencer method to variations in audio input, suggesting that it is not overfitting to specific audio features.

For the starting portrait, we conducted experiments on 50 different portraits of CelebA-HQ in Table 1. The average sync value is 3.9685 and the standard deviation is 1.5607. Our findings indicate that the effectiveness of adversarial perturbations varies across different facial identities, sug-

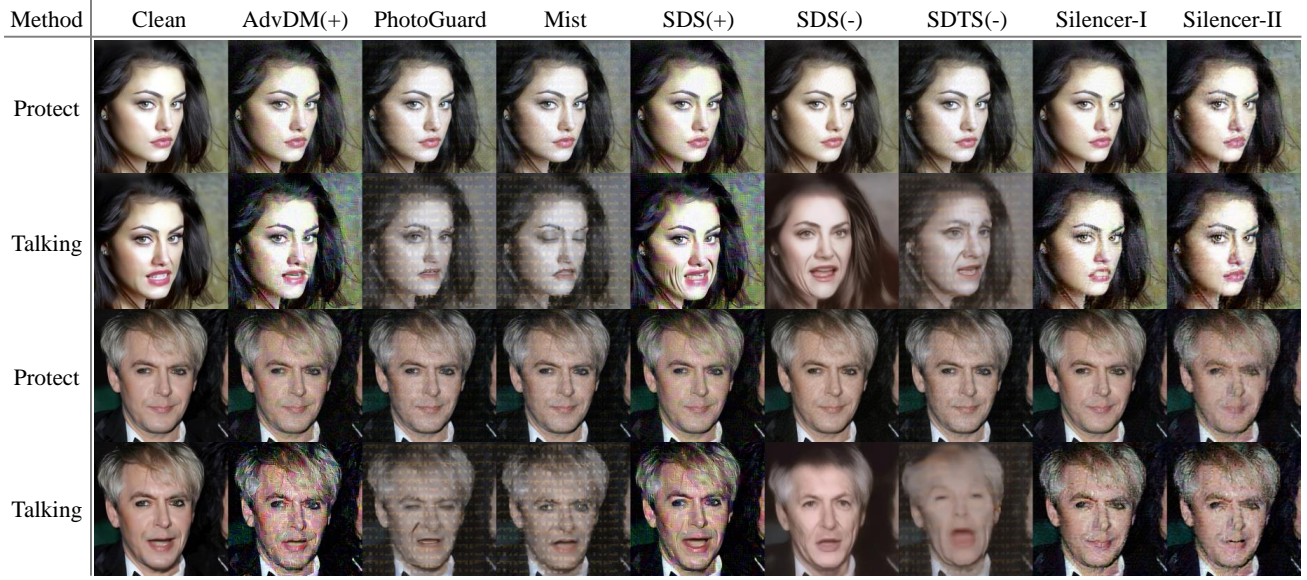


Figure 10. Additional Visualization Comparison with Image Protection Methods in CelebA-HQ [25].

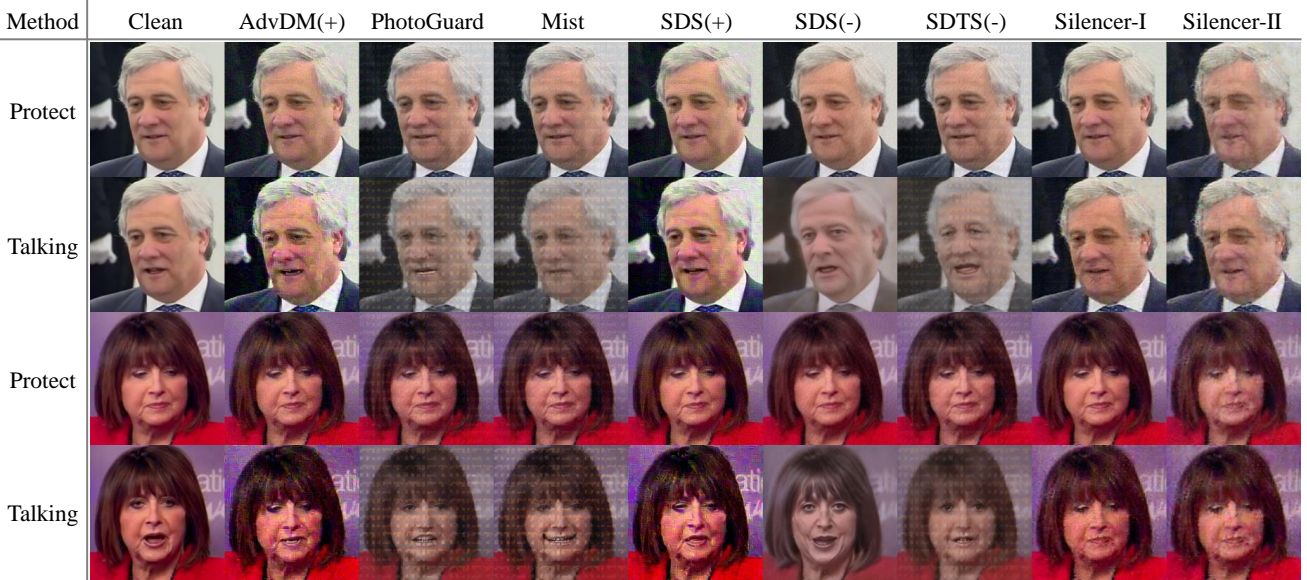


Figure 11. Additional Visualization Comparison with Image Protection Methods in TalkingHead-1KH [53].

gesting variations in inherent robustness. We intend to investigate the factors contributing to this variability in future research.

Ablation Study on Perturbation Budget in Silencer-I.

To understand the influence of the perturbation budget on the effectiveness of Silencer-I, we conducted an ablation study on the CelebA-HQ dataset. Specifically, we investigated the performance of Silencer-I under constrained l_{inf} perturbation budgets. The l_{inf} limits the maximum change

allowed for any single pixel value in the input image. A smaller budget implies a more subtle, less perceptible adversarial perturbation. As shown in Table 10, we evaluated Silencer-I with two different l_{inf} budget: 8/255 and 16/255. The results demonstrate that decreasing the perturbation budget leads to a reduction in Silencer-I’s performance. This is because a smaller budget restricts the degree to which Silencer-I can modify the input image to disrupt synchronization. However, even with a stricter budget, Silencer-I still achieves a notable level of protection perfor-

mance compared with existing methods in Table 1. This suggests that Silencer-I is more effective, achieving considerable protection with fewer changes to the input portrait.

Ablation Study on Inverted Timesteps in Silencer-II.

We conducted an ablation study on the inverted latent space timesteps used in Silencer-II. Due to memory constraints, we investigated the impact of optimizing the latent feature for the final timestep versus optimizing for the final two timesteps specifically in the context of DDIM inversion. As shown in Table 11, optimizing the latent feature at only the final timestep yielded superior performance while consuming fewer resources compared to optimizing the last two steps. Consequently, we opted for the single-timestep optimization strategy. Further exploration is needed to improve the efficiency and effectiveness of latent feature optimization, addressing potential vulnerabilities to purification methods.

Ablation Study on \mathcal{L}_T in Silencer-II. We perform an ablation study to evaluate the effectiveness of \mathcal{L}_T in optimizing the inverted latent representation. As shown in Fig. 8, while the nullifying loss \mathcal{L}_N still produces disturbed results, it achieves this by distorting the portrait, compromising the output’s quality and identification. It is mainly because the talking-head model fails to operate effectively when it cannot detect a face, rendering it unable to function as intended. This highlights the necessity of exploring optimized solutions that protect privacy without sacrificing visual integrity. With the assistance of \mathcal{L}_T , we can effectively reduce noise in the facial region while achieving our intended objectives. This approach strikes a balance between minimizing distortions and achieving the desired outcomes, enhancing the overall effectiveness of Silencer.

Ablation Study on the Initial Iteration s without Mask in Silencer-II.

To prevent facial blurring, we incorporate a face mask during the training process of Silencer-II. We begin by training the entire image without a mask for s iterations. Subsequently, a face mask is applied to exclude the facial region from further optimization. To verify the effect of s , we conduct an ablation study on a subset of CelebA-HQ, as shown in Fig. 9 and Table 12. The results indicate that as the number of iterations s increases, face quality deteriorates while protection performance improves. Therefore, we set $s = 100$ in our main experiments as it offers a balanced trade-off between maintaining facial clarity and achieving effective protection.

A.5. Additional Visual Results

Additional qualitative comparisons are presented in Fig. 10 and Fig. 11. These figures illustrate that our Silencer consistently achieves superior protection performance across

various datasets. These video results can be found in our supplementary video.